Interfacial-roughness effects on giant magnetoresistance and interlayer coupling in Co/Cu superlattices

Z. J. Yang and M. R. Scheinfein
Department of Physics and Astronomy, Arizona State University, Tempe, Arizona 85287-1504
(Received 27 February 1995; revised manuscript received 28 April 1995)

Giant magnetoresistance and interlayer exchange coupling in Co/Cu superlattices grown by *e*-beam evaporation have been investigated by using the combined three-axis magneto-optical Kerr effect, magnetotransport measurements, x-ray diffraction, Rutherford backscattering, transmission electron microscopy (TEM), and domain observation with scanning transmission electron microscope electron holography. Large-angle x-ray scattering data and TEM images indicate that the superlattices have fcc (111) orientation with polycrystalline grain sizes ranging from 10–14 nm. Small angle x-ray scattering and cross-section TEM images show that the superlattices have a well-defined layer structure, coherent grain-to-grain epitaxial growth, and interfacial roughness of ± 0.2–0.4 nm. The correlations between the 90° magnetization and magnetoresistance oscillation curves suggest that the giant magnetoresistance in superlattices with imperfect interfaces results from the 90° orientation of domains within adjacent Co layers.

I. INTRODUCTION

The discovery that the exchange coupling across nonmagnetic spacer layers in a wide variety of ferromagnetic transition-metal superlattices can oscillate between antiferromagnetic (AF) and ferromagnetic (*F*) as a function of the interlayer thickness has attracted considerable attention from both the fundamental and application viewpoints. The strength and sign of the interlayer coupling coefficients in superlattices have been correlated with magnetotransport measurements for a wide class of systems.[1–5] Experiments have been focused on the bcc Fe/Cr (Refs. 6-8) and the fcc Co/Cu systems[4,9–12] in an effort to confirm quantitative predictions on the orientation dependence of the interlayer coupling.[11–17] Magnetotransport models which rely on antiferromagnetic alignment of adjacent ferromagnetic layers have been used to interpret experimental data.[18–22] Interlayer coupling can be complicated by surface and interface roughness, primarily due to conditions during growth.[23–26] In addition to antiferromagnetic (180° or bilinear) interlayer coupling, 90° (or biquadratic) interlayer coupling has been observed in epitaxial systems with wedge-shaped interlayers, including Fe/Cr/Fe(100) and Fe/Au/Fe(100).[27–30] At least three types of mechanisms may give rise to biquadratic coupling.[31] The first is associated with spatial fluctuations of bilinear coupling due to terraced variations of spacer thickness in nonideal specimens.[32,33] The second in the intrinsic mechanism in which biquadratic coupling arises from the electronic structure of an ideal trilayer.[34–36] The third is the loose-interfacial-spin mechanism,[31] where each interfacial layer of magnetic atoms is weakly exchange coupled to the remainder of the ferromagnets, and the observed biquadratic coupling is intrinsic rather than due to impurities or structural defects. Intrinsic bilinear (180°) coupling in general coexists with the higher-order biquadratic (90°) coupling.[29] Evidence for 90° domains in the coupling in Co/Cu(001) superlattices has been recently observed in the nonsymmetric spin states from Kerr hysteresis loops at the second antiferromagnetic maximum[37,38] due to the competing effects of anisotropy and exchange coupling. Elemental specific magnetic hysteresis loops extracted from magnetic circular dichroism experiments from Fe/Cu/Co trilayers indicates the presence of significant misalignment between the orientation of the magnetization in adjacent ferromagnetic layers.[39] The strong correlation between giant magnetoresistance (GMR) and 90° domain formation between adjacent layers in electron-beam-evaporated Co/Cu superlattices as a function of the Cu interlayer spacing has been found when the interfaces are imperfect.[38] In this paper, interfacial roughness effects on giant magnetoresistance and interlayer coupling in Co/Cu superlattices are studied systematically with microstructural and magnetic characterization, magnetotransport measurements, and magnetization reorientation modeling.

II. EXPERIMENT

A. Structural characterization

A series of $[Co_{1.5\ nm}/Cu_t]_n$ $(7 < a < 13)$ superlattices have been prepared by evaporating on Si(100) oriented crystals, Corning cover glass slides, and holey carbon film covered grids. 6.0 nm thick Co layers were grown at 250 °C as buffer layers on the substrates. Our experiments on modifying the substrate temperature during deposition suggest that the optimum temperature for the first buffer layer is about 250 °C and 150 °C for the superlattice stack. The use of a buffer layer gave the best GMR properties.[40] Scanning transmission electron microscopy (STEM) and large-angle x-ray scattering (LAXS) results from pure Co thin films indicate that the 6.0 nm thick Co buffer layer will lead to flat Co and Cu layers. 4.5 nm thick Co capping layers covered the superlattices, making the sandwich symmetric. The total

superlattice thickness ranged between 40 and 46 nm, sufficiently thin so as to be electron transparent to the 100 keV electron beams used to characterize the magnetic microstructure with electron holographic methods. All films were grown at room temperature in a dual *e*-beam UHV evaporation system. Deposition rates were 0.3–1 Å/s at a base pressure 5×10^{-9} mbar. A growth pressure of 5×10^{-8} mbar can be maintained with a low growth rate of 0.3 Å/s. *In situ* thickness calibration using a quartz crystal microbalance was confirmed with Rutherford backscattering (RBS).

The crystallographic and superlattice structure was studied with RBS, x-ray diffraction (Cu $K\alpha$ radiation $\lambda=0.1504$ nm), and plane view STEM. RBS data and theoretical fits assuming bulk densities for Co and Cu and no interface mixing for a test multilayer structure consisting of four Co layers 9 nm thick separated by four Cu spacers 9 nm thick indicate a well-defined superlattice structure.[41] The incident ^{4}He beam energy was limited to 2 MeV, and was recorded with the total 1024 scanning channels. A grazing incidence geometry was used for the observation of the modulation due to the superlattice structure.

The x-ray spectra were measured using a Rigaku D/Max-II diffractometer with $K\alpha$ radiation from a fixed Cu anode. The $\theta-2\theta$ scan speed was typically 0.5°/s with steps of 0.004° for small-angle x-ray scattering (SAXS) and 4°/s with steps of 0.02° for LAXS. The LAXS data, as shown in Fig. 1, are characterized by a fcc (111) Co (Cu) peak indicating that the multilayers have a (111) out-of-plane texture. Some films show a very weak fcc (200) Co (Cu) peak. The peak positions shifted slightly from the fcc (111) Co peak position ($2\theta=44.2°$) towards the fcc (111) Cu peak position ($2\theta=43.5°$) as the Cu spacer thickness increases. Figure 2 shows the spacing $d_{\langle111\rangle}$, calculated from LAXS peak positions for all films, vs the Cu spacer thickness t_{Cu}, showing $d_{\langle111\rangle}$ increases as the Cu spacer thickness increases, but never reaches the bulk fcc Cu(111) value (2.078 Å). For example, in the 2.0 nm thick Cu spacer sample, $d_{\langle111\rangle}$ is about 2.07 Å, indicating that the structure of the multilayer is neither that of bulk Cu nor that of bulk Co. Rather, it is a strain-modified fcc Co/Cu(111) superlattice structure.

The grain sizes can be calculated from the half-width of the Bragg peak by using the Scherrer equation:[42]

$$L=\frac{K\lambda}{\beta\cos\theta}\ , \tag{1}$$

where θ and λ are diffraction-angle and x-ray wavelength, L is the mean dimension of the grains, β is the full width at half intensity (FWHI) of the interference peak in radians and K is a constant approximately equal to unity and related to the crystal; for crystallites in platelet form, K equals 0.89. The average grain sizes of the films calculated from Eq. (1) range between 10 and 14 nm. The FWHI β of the fcc (111) peak decreases from 0.8° to 0.6° as a function of increasing Cu interlayer thickness, indicating an increase in grain size and fewer defects in the layer structures because of a smaller number of grain boundaries.

SAXS profiles of the superlattices are shown in Fig. 3.

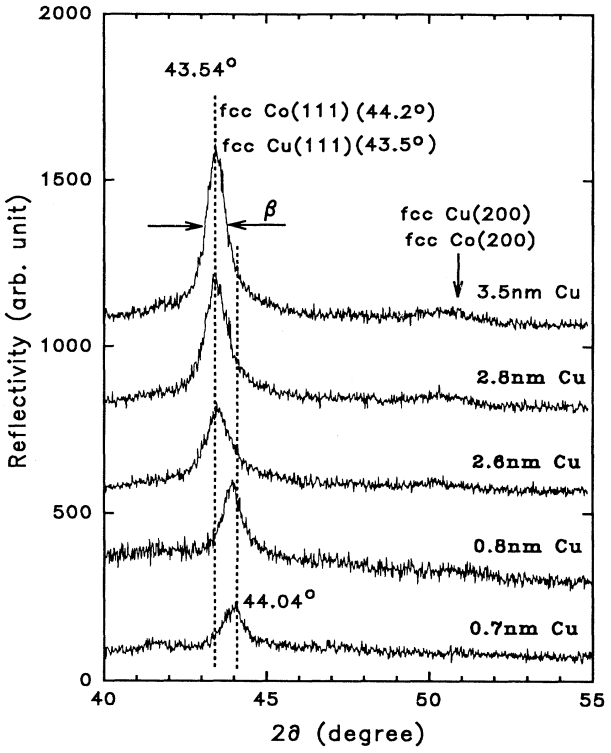

FIG. 1. Large-angle x-ray scattering data from superlattices of Si/Co (6 nm)/[Cu(t_{Cu})/Co (1.5 nm)]$_n$; n, the bilayer number, is between 6 and 13. The Cu spacer thickness of all films and the fcc Co and fcc Cu are marked. The FWHI β of the fcc (111) peak is decreasing as a function of Cu interlayer thickness.

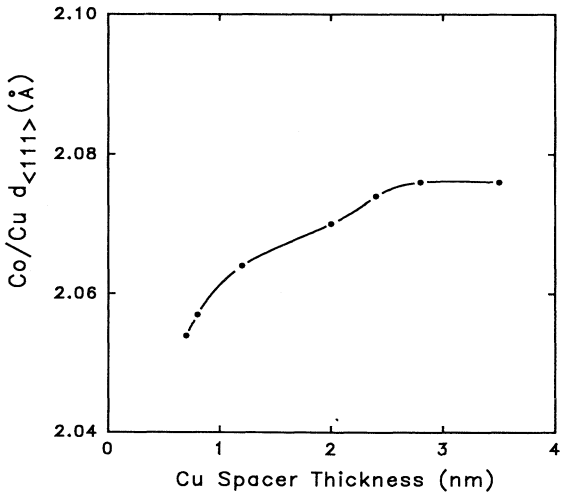

FIG. 2. Atomic plane spacing $d_{\langle111\rangle}$ vs the Cu spacer thickness (note that in pure Co and pure Cu crystal, $d_{\langle111\rangle Co}=2.048$ Å, $d_{\langle111\rangle Cu}=2.078$ Å) in the series of superlattices Si/Co (6 nm)/[Cu(t_{Cu})/Co (1.5 nm)]$_n$ ($6<n<13$), calculated from LAXS data.

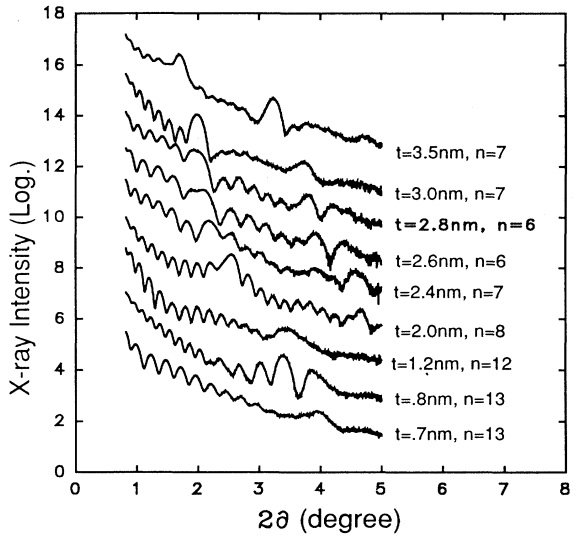

FIG. 3. SAXS profiles for the series of Si/Co (6 nm)/[Cu(t_{Cu})/Co (1.5 nm)]$_n$/Co (4.5 nm) multilayers. The Cu interlayer thickness and the number of bilayers are marked for each film.

Only first-order SAXS Bragg peaks with superlattice character Kiessig fringes were observed for the films with Cu interlayer thickness thinner than 1.2 nm, indicating the presence of relatively rough interfaces and wavy layers. The rms roughness of the interface estimated by fitting the SAXS spectra is ± 0.2–0.4 nm. In Fig. 4, the SAXS profile of the Si/Co (6 nm)/[Cu (2 nm)/Co (1.5 nm)]$_8$/Co (4.5 nm) film is shown, together with an offset (for clarity) SAXS spectrum calculated with a standard dynamical scattering model.[43–45] In order to model the spectral structures and damping rate, the interface roughness and layer spacing have to be correctly defined. The fits were simulated with a 2.0 nm silicon oxide layer between the Si substrate and the very first Co buffer layer, a 4.5 nm topmost rough CoO layer, and an interface roughness of ± 0.2 nm for the lower half of the superlattice stack, and ± 0.4 nm for the top half.

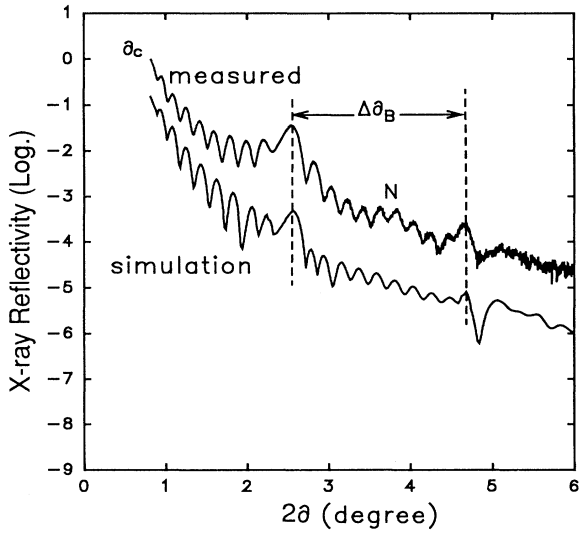

FIG. 4. SAXS profiles of the superlattice with the structure of Si(100)/Co (6 nm)/[Cu(2 nm)/Co (1.5 nm)]$_8$/Co (4.5 nm). The top profile is measured data, and the lower one is the simulation with the parameters given in the text.

The observed broadening of the higher-order Bragg peaks and the disappearance of the high-order low-angle amplitudes may arise from interfacial interdiffusion and cumulative random variations in layer thickness.[46] Our LAXS and SAXS results indicate that the films grown on Si substrates have better crystalline orientation and are smoother than those grown on glass substrates,[47] but as the Cu interlayer gets thicker, the difference seems to decrease.

Characterization methods based on the transmission electron microscope (TEM) enable the local microstructure of a material to be visualized directly in a manner that is not possible with bulk techniques such as x-ray diffraction and Rutherford backscattering.[48] Figure 5(a) shows a 200 kV transmission electron micrograph at large overfocus ($\sim$200 nm) showing compositional layering from the multilayer with a nominal structure Si(100)/Co(6 nm)/[Cu (2 nm)/Co (1.5 nm)]$_8$/Co (4.5 nm). The sample was cross sectioned such that the direction of observation would be parallel to the substrate surface and along the [110] zone axis.[49] Diffraction contrast and defocusing techniques[48–51] were used to study the presence

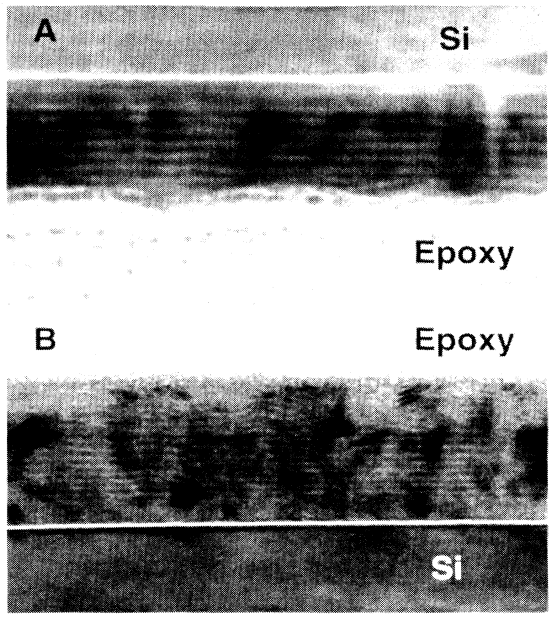

FIG. 5. (a) Cross-section transmission electron micrograph of Co/Cu multilayer with nominal structure Si(100)/Co (6 nm)/[Cu (2 nm)/Co (1.5 nm)]$_8$/Co (4.5 nm). The brightest layer is native oxide SiO, the top of the image is Si substrate, and the bottom is epoxy mount. The dark layers are Cu spacer layers. (b) Cross-section transmission electron micrograph of Co/Cu multilayer with nominal structure Si(100)/Co (6 nm)/[Cu(0.8 nm)/Co (1.5 nm)]$_{13}$/Co (4.5 nm), illustrating a wavy layered structure when the Cu spacer layer is very thin.

of texturing and long-range orientational relationships. The successive layers of native oxide SiO (~3 nm), Co buffer layer (~6 nm), Co/Cu multilayer, and epoxy mount can be distinguished, illustrating clearly that the superlattice structures have sufficient quality to maintain separation of the layers. The long vertical structures that penetrate the superlattice are crystallites, so there is some texturing confirmed by x-ray-diffraction data. The flatness and continuity of the layers in these micrographs does not indicate any obvious pinhole formation,[52] although it does not rule out pinhole formation given the averaging in TEM cross-section imaging. High-resolution electron micrographs recorded at optimum defocus show epitaxy at the Co/Cu interfaces. The grain size of the Co buffer layer is about 10 nm in diameter, and it propagates into the multilayer by grain-to-grain epitaxy.[49] The atomic layers are coherent over several hundred Å, which again is consistent with our x-ray-diffraction data. The GMR and AF coupling effects were first found[1,50] in Fe/Cr and Co/Cu epitaxial multilayers fabricated by molecular beam epitaxy (MBE). By contrast, polcrystalline superlattices deposited by simple techniques such as sputtering and evaporation have introduced questions about the influence of grain size, morphology, orientation, and texture on the magnetoresistance effect and magnetotransport mechanism. Interface and bulk scattering at grain boundaries are likely to be important in GMR superlattices.[51] Figure 5(b) shows a TEM image of the superlattice with a nominal Cu interlayer thickness of 0.8 nm, illustrating a wavy layer structure. The rms interface roughness has been estimated from the lines scans of the TEM images. The values extracted from the TEM data agree well with the values extracted from the SAXS simulations.

B. Magnetic characterization

The Co/Cu multilayers are well characterized layered structures with interface roughness of ± 0.2–0.4 nm, fcc (111) texturing, average grain size of 10 nm, and grain-to-grain epitaxial coherence. In order to investigate the origin of the GMR and magnetic coupling in these superlattices, a study[38] of the magnetic alignment within adjacent Co layers has been carried out with the combined three-axis magneto-optical Kerr effect (MOKE). The combined longitudinal-transverse Kerr intensity for our MOKE measurements can be expressed as[53]

$$I \cong m_l^2 (r_{ps}^l)^2 + 0.2 m_l r_{pp}^l r_{ps}^l \sin(\delta_{pp}^l - \delta_{ps}^l) \sin\omega t \ , \qquad (2)$$

where m_l is the direction cosine of the magnetization axes along the applied field direction (projection of M and H) for the longitudinal Kerr effect. r_{ps}^l and δ_{ps}^l are the absolute magnitude and phase angle of the Fresnel reflection coefficients [superscripts indicate (p) polar or (l) longitudinal effects], and ω is the angular frequency of the modulator. For our experimental configuration,[53] the expression for the intensity is independent of the transverse Kerr effect, regardless of the direction of the applied magnetic field. The longitudinal in-plane component of the magnetization M_x is obtained from longitudinal Kerr effect hysteresis loops, measured from 6 mm diameter circular samples by orienting the superlattice's in-plane easy axis along the applied magnetic-field direction in the scattering plane. In order to obtain the transverse in-plane component of the magnetization, M_y, both the sample and the magnetic field are rotated until both the easy axis and the applied field direction are perpendicular to the scattering plane. Without modifying the position of any optical elements, calibrated M_x and M_y components of the magnetization can be recorded during the switching process. This allows us to measure both in-plane magnetization components M_x (the component along the longitudinal direction) and M_y (the component along the transverse direction) from the same longitudinal MOKE effect. The components can be added together in quadrature as a measure of the total magnetization, M_s. When the normalized total magnetization differs from one, there are regions where the magnetization is misaligned. The misalignment can be due to domain formation within a given layer(s) of the superlattice, or may be due to small regions of antialignment between adjacent layers. As the light is attenuated during its traversal of the superlattice, the topmost layers will contribute more strongly to the detected Kerr signal.[54] It has been shown that the interfaces between Co and Cu get rougher with increasing distance from the substrate surface.[55] In order to assess effects due to cumulative roughness in layered structures, Kerr effect hysteresis loops were measured from both sides of samples grown on glass substrates. No obvious difference was observed in hysteresis loops measured from the top or the bottom of the superlattice stack. The variation in the absolute value of the Kerr signal as samples are changed and the magnet and sample are rotated is less than 5%.

The magnetoresistance (MR) was measured on both strip-shaped (5×8 mm^2) and patterned, dumbbell-shaped (5×0.2 mm^2) samples using the four-probe method at 300 and at 77 K with the field (up to 14 kOe) applied in the plane of film, and the in-plane current both transverse and parallel to the field. We define MR as $(R_H - R_{\rm sat})/R_{\rm sat}$, where $R_{\rm sat}$ is the saturation high-field resistance.

In Fig. 1 of Ref. 38 we showed the magnetoresistance at room temperature and at 77 K as a function of the Cu interlayer thickness for the superlattice Si(100)/Co (6 nm)/[Cu (2 nm)/Cu(t)]$_n$/Co (4.5 nm) ($6 < n < 13$). The interlayer coupling oscillation period was about 1 nm. The first MR maximum was suppressed and the value for the MR was reduced,[4,9,10,38] characteristic of films with roughness large enough to produce pinhole coupling for such thin Cu layers.[23–25,38] The maximum normalized magnetization oriented at 90° with respect to the field direction, M_y (or $M_{90^\circ}/M_{\rm sat}$), was also shown. The peaks in the 90° oriented magnetization correspond with the peaks in the magnetoresistance data at approximately $t_{\rm Cu}$ of 0.8, 2.0, and 2.8 nm. 90° domain orientation is still present at the first oscillation maximum even though the value of the MR is strongly suppressed.[38]

In order to illustrate the correlation between 90° coupling and MR in superlattices with rough interfaces, the two in-plane components of the magnetization extracted from longitudinal and "transverse" Kerr effect hysteresis loops were shown for selected films in Fig. 2 of Ref. 38 as a function of the normalized field. In all films examined, H_c (here $2H_c$ is the width of the hysteresis loop along the $M=0$ axis) was approximately 30 Oe. Using these results, the interlayer coupling for t_{Cu} 0.7 nm and 1.0 nm is seen to be ferromagnetic. This conclusion is verified by the squareness of the hysteresis loops and the very small amount of magnetization M_y perpendicular to the easy axis during reorientation. The resulting MR is small and comparable to the transverse MR results from pure Co films. The typical interpretation of hysteresis loops at the first and second oscillation maxima indicates antiferromagnetic coupling.[1-10,18-25] In the case of rough interfaces, the stepped, compound easy-axis hysteresis loops resulting from antiferromagnetic coupling are not observed.[39] Rather, the easy-axis hysteresis loops, M_x, are canted and rounded. However, during the switching process, the magnetization reorients itself along a direction 90° from the easy axis and the field direction. This is clear evidence that there is 90° domain formation in the superlattice which appears as 90° coupling.

We have found that the coercivity H_c in some of our Co/Cu superlattices with very thin Cu spacer layers is slightly larger than the field position H_m at the MR curve peak. In contrast, to within the accuracy of our measurements, in the sample having the largest GMR value with the structure of [Cu (2 nm)/Co (1.5 nm)]$_n$ and the samples with thicker Cu spacer layers, the MR maximum occurs at H_c. Compared with the results from our pure Co thin-film experiments which show that H_c is always larger than H_m in all films, we would like to conclude that those superlattices with thin Cu spacer layers show some pure thin-film behavior.

Should antialignment between domains within the layers or between the layers themselves be present, then the quadrature sum of the magnetization during the switching process should not be constant. Within the accuracy of our Kerr effect measurements, some regions of magnetization are misaligned with each other.[38] The switching is not solely due to coherent rotation since little hard-axis magnetization M_y is detected in the ferromagnetically coupled superlattices. In all cases studied here, there is no correlation between the percentage of misalignment, extracted from the magnitude of the dip in the M_s values, and the percentage of MR. The field values at the position of the MR maxima and the M_s minima are almost the same. In all cases, the estimated change in M_S from saturation to H_c due to slope in the easy-axis hysteresis loops is less than 1%. Hence we conclude that the MR is correlated with 90° (with respect to the field and easy axes) orientation of domains or layers within the superlattice.

Accurate quantitative micromagnetic structure determined by STEM electron holography[56,57] can be used to address the issue of whether or not the domains are magnetically coupled throughout the entire superlattice.[58]

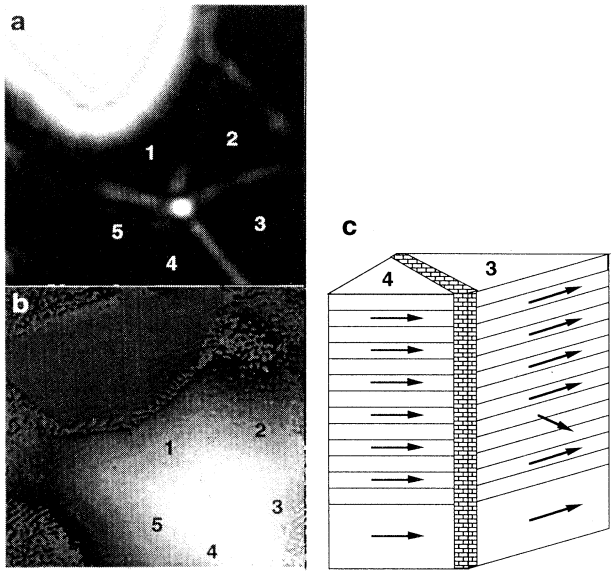

FIG. 6. Domain structure for the superlattice with a nominal structure of Co(6 nm)/[Cu (3 nm)/Co (1.5 nm)]$_6$/Cu(3 nm)]. (a) Fresnel image (2.8 μm across). The domains are numbered 1–5, respectively. (b) Absolute mode STEM electron holographic phase image; (c) A proposed domain structure in the region of the superlattice imaged in (a), indicating the presence of 90° domain formation within the superlattices stack, and the presence of domains within the layers themselves.

Figure 6(a) shows a Fresnel image (2.8 μm across) for a superlattice with a nominal structure of Co (6 nm)/[Cu (3 nm)/Co (1.5 nm)]$_6$/Cu(3 nm), taken at remanence. The large white area in the upper left of Fig. 6(a) is a hole in the film. This enables us to perform absolutely calibrated magnetization measurements in this region of the film. Fresnel images show domain walls as either white or black lines. The regions between the walls are the domains. In Fig. 6(b), an absolute mode electron holographic phase image is shown, once again, in zero field. The maximum slope of the phase within an in-plane oriented domain absolutely determines the thickness-averaged magnetization.[56] The magnitude of the saturation magnetization can be typically determined to better than 2% if the ferromagnetic film thickness is known.[56] We use the absolute calibration in the phase image shown in Fig. 6(b) to extract the in-plane component of the magnetization within each domain. Assuming a bulk saturation magnetization of Co (18.17 kOe), the calculated maximum phase gradient for domains uniformly magnetized to saturation and penetrating the whole stack should be 0.0414 rad/nm. The maximum phase gradients of the domains 1, 2, 4, and 5 are 0.041 ± 0.0006 rad/nm, indicating that the domains penetrate the stack and are uniformly (ferromagnetically) aligned. The phase gradient of domain 3 is 0.0367 rad/nm, which is 10% less than the uniformly magnetized value. If a single layer were antiferromagnetically aligned within this domain, the phase

gradient would have to be 20% lower. Therefore, the magnetization in one of the layers (10% of the active thickness) is rotated 90° with respect to the magnetization in the other layers. A proposed domain structure in the region of the superlattice imaged in Figs. 6(a) and 6(b) is shown in Fig. 6(c), indicating the presence of 90° domain formation within the superlattice stack, and the presence of domains within the layers themselves.[57] This is strong evidence to support the results of our Kerr effect magnetic hysteresis loop measurements and magnetotransport measurements. No apparent correlation between antiferromagnetic alignment (as extracted from total magnetization curves) and GMR was observed, indicating that the GMR was due to 90° alignment of adjacent layers or domains.

III. INTERLAYER COUPLING AND MAGNETOTRANSPORT MECHANISMS

The correlations between the 90° magnetization curves and magnetoresistance measurements suggest that the giant magnetoresistance in superlattices with imperfect interfaces results from the 90° orientation of domains within the superlattice stack and the presence of domains within the layers themselves. A much-debated issue concerns the appearance of GMR in samples that show little[59–62] or no[63,64] evidence of antiferromagnetic interlayer coupling. It has been suggested that AF interlayer coupling may be masked in the Co-Cu (111) system by stacking faults[65] and pinholes,[9] and 90° coupling may arise from spatial nanoscopic fluctuations in the interlayer coupling through the nonmagnetic spacer layer.[32,33] Erickson and co-workers[34,35] calculated the bilinear (or 180°) interlayer coupling constant A_{12} (J_{AF}) and the biquadratic (or 90°) interlayer coupling constant B_{12} based on a free-electron model and found that both A_{12} and B_{12} oscillate with spacer-layer thickness. The overall amplitude of B_{12} is generally smaller than that of A_{12}. The criterion for biquadratic coupling is $B_{12} > |A_{12}|$. This may happen at the nodes of the A_{12} oscillation curves when A_{12} is near zero at certain regions of spacer-layer thickness. It has been pointed out[19] that the AF coupling is sufficiently strong to overcome random coercive or pinning forces that oppose realignment within the magnetic layers only for ideal (perfect) layer structures. However, near the nodes where the AF couplings goes through zero and for large spacer thickness, the AF coupling is no longer strong enough compared to the pinning forces to define uniquely the magnetic configuration of the multilayers. Almost all theoretical approaches to AF interlayer coupling are based on the assumption that the layers are atomically flat, whereas real samples always have some interfacial roughness.

The switching behavior of the superlattice can be analyzed most simply as the coherent rotation of two exchange-coupled, layers with magnetocrystalline anisotropy, external magnetic field, and interlayer coupling energies.[66] In order to incorporate roughness into this simple model, a parameter which describes the percentage of the films that are antiferromagnetically coupled is included. Phenomenologically, the total energy of a superlattice, with magnetic layers having identical thickness t and area A, can be written in dimensionless form as

$$\frac{E}{2k} = -\frac{H_x}{H_k}(\cos\theta_1+\cos\theta_2) - \frac{H_y}{H_k}(\sin\theta_1+\sin\theta_2)+\tfrac{1}{2}q(\theta_1,\theta_2,\beta) + \frac{H_{ex}}{H_k}[a-p(1-a)]\cos(\theta_1-\theta_2)\ , \tag{3a}$$

and

$$q(\theta_1,\theta_2,\beta)=\begin{cases}\tfrac{1}{2}[\sin^2 2(\theta_1-\beta)+\sin^2 2(\theta_2-\beta)]\ , & \text{cubic}\\ [\sin^2(\theta_1-\beta)+\sin^2(\theta_2-\beta)]\ , & \text{uniaxial}\end{cases} \tag{3b}$$

where only three free parameters exist; p ($|J_F/J_{AF}|$), the ratio of the ferromagnetic to antiferromagnetic interlayer coupling strength, a, the percentage of the films that are antiferromagnetically coupled, and H_{ex}/H_k, the normalized interlayer exchange field representing the competition between the exchange energy and anisotropy energy. Here, E is the energy density per unit volume, $\theta_{1,2}$ are the angles in layers 1 and 2 relative to the x axis, β is the in-plane easy axis orientation, H_x and H_y are the two components of the applied in-plane magnetic field, $H_k = 2k/M_s$ is the anisotropy field (k is an effective bulk-like anisotropy averaged over the film thickness[67]), and $H_{ex} = J_{AF}/tM_s$ is the interlayer coupling field (here, M_s is the saturation magnetization). We do not consider the intrinsic 90° interlayer coupling here mainly because the biquadratic coupling constant B_{12} calculated from the free-electron model is too small when compared with A_{12}.[34] The equilibrium conditions can be obtained by minimizing the energy using a conjugate gradient method. No biquadratic exchange energy terms are necessary to have equilibrium magnetization directions in the layers at right angles to each other during the switching processes.

In order to estimate the range of the interlayer coupling values needed in the simple coherent rotation model outlined above, we convolve the interfacial roughness of $\sigma \approx \pm 0.2$–0.4 nm extracted from TEM and SAXS data with the ideal interlayer coupling data.[16] We use the theoretical data from Ref. 16 calculated for the fcc Co-Cu (001) system ($\Lambda \approx 2.56$ and 5.88 ML for short and long oscillation) at $T=0$ and interfacial roughness $\sigma=0$. For a Gaussian distribution of interfacial roughness, the intensity and period of the interlayer coupling are to be modulated by convolution with a Gaussian function as

$$A_{12}(t,\sigma)=(\sigma\sqrt{2})^{-1}\int A_{12}(\xi-t)\exp(-\xi^2/2\sigma^2)d\xi\ , \tag{4}$$

where t is the spacer-layer thickness. Figure 7(a) shows results of the convolution where the solid line is the theoretical data from Ref. 16 for an ideal fcc Co/Cu superlattice, and A_0 is about 13 erg cm^{-2}. It can be seen

clearly that the period of oscillation spreads out and the intensity of AF coupling is diminished as the roughness increases. The intensity of the coupling for an rms roughness of 0.2 nm is only 20% of that compared to the theoretical curve representing perfect layers with zero roughness. At this roughness (0.2 nm), very weak AF coupling appears at the Cu spacer thicknesses of 0.9, 2.0, 3.0, and 4.0 nm, as shown in the expanded view of Fig. 7(b). This period is consistent with the accepted range of Cu spacer thicknesses indicating that the interfacial roughness and incomplete AF coupling should be considered in interpreting experimental data reported for Co/Cu superlattices. This weak AF coupling is totally masked at the roughness of 0.4 nm leaving the possibility for 90° coupling. Only after the interlayer AF (180°) coupling is masked by interlayer roughness does the 90° coupling (in the strict sense, 90° orientation of domains within superlattice stack and the presence of domains within the layers themselves) arising from interfacial roughness become dominant. This is indicated in the magnetic phase diagrams in Fig. 8. Here, coupling regimes are extracted from hysteresis loops generated with the coherent rotation model expressed in Eqs. (3). Regions are specified by the type of coupling present at the coercive field as I (ferromagnetic), III (antiferromagnetic), and II (90°). In Figs. 8(a)–8(c), cubic in-plane anisotropy was assumed, while in Fig. 8(d), in-plane uniaxial anisotropy was selected. The values of H_{ex}/H_k are 3, 2, and 1 in Figs. 8(a), 8(b), and 8(c), respectively. In the uniaxial case, Fig. 8(d), $H_{ex}/H_k=1$. All coupling phase diagrams, obtained from simulations with in-plane fourfold anisotropy, show three coupling regions shifted from left to right as the H_{ex}/H_k decreases, indicating the competition among anisotropy, interlayer exchange coupling, and external field energy.[66,68] Only a narrow region of very weak antiferromagnetic coupling exists when anisotropy is dominant ($H_k > H_{ex}$). This narrow antiferromagnetic coupling region totally disappears when $H_k \gg H_{ex}$, while 90° coupling always coexists with ferromagnetic coupling for the fourfold anisotropy case. When uniaxial anisotropy is dominant, the 90° coupling region as extracted from the coherent rotation model disappears, as shown in Fig. 8(d). A distribution of fourfold easy axes can be used to describe the anisotropy of our Cu/Co superlattices. For our films, $H_c \approx 35$ Oe. In a coherent rotation model, the switching field for in-plane cubic anisotropy is typically 60% of $2k/M_s$, hence, $H_k \sim 60$ Oe. This yields a value of $J_{AF}=0.039$ erg/cm^2. Based on this crude model, this value is in reasonable agreement with the published data for the Co/Cu system.[67] The structure of the coupled hysteresis loops for the three regions is shown schematically in Figs. 9(a)–9(i) (with a distribution of in-plane

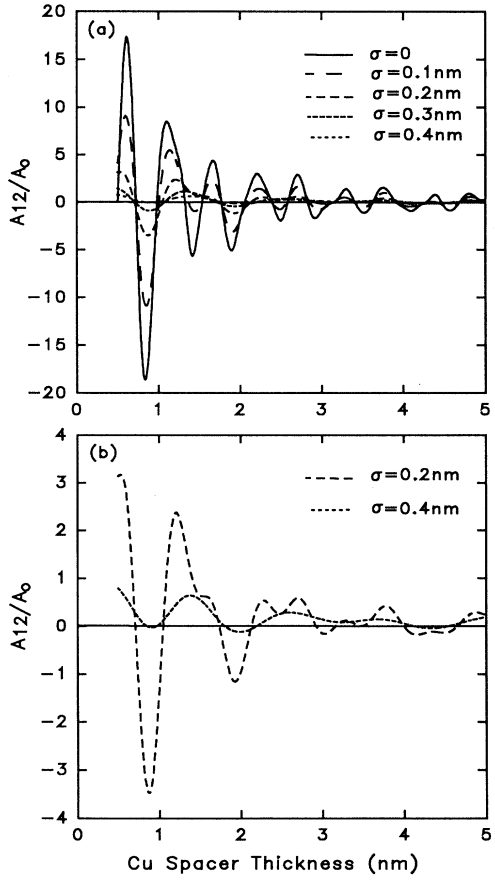

FIG. 7. Oscillation curves of AF interlayer coupling constant A_{12} (normalized to A_0) with different roughness for (a) fcc Co-Cu multilayers as a function of the Cu spacer thickness showing that the intensity is diminished and the period modified as the roughness increases. (b) A_{12} with a roughness of 0.2 nm is only 20% of zero roughness coupling constant, and this weak AF coupling is almost totally masked with a roughness of 0.4 nm.

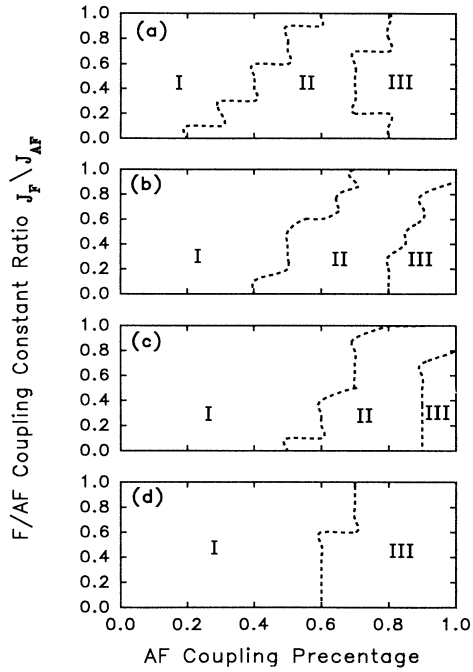

FIG. 8. Magnetic coupling phase diagram of stable orientations (see text). (a) $H_{ex}/H_k=3$, (b) $H_{ex}/H_k=2$, and (c) $H_{ex}/H_k=1$, with a distribution of in-plane fourfold anisotropy. (d) The case of in-plane uniaxial anisotropy with $H_{ex}/H_k=1$.

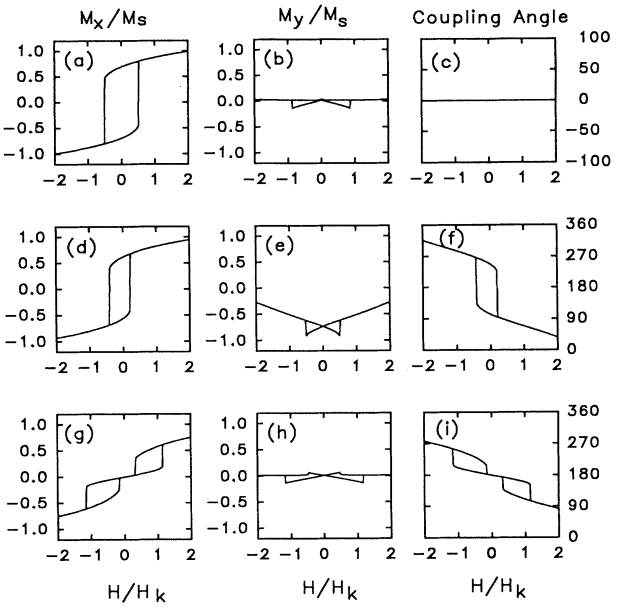

FIG. 9. Compound longitudinal hysteresis loops and interfilm coupling angle between two adjacent ferromagnetic layers during switching processes ($H_{ex}/H_k=3$ and $J_F/J_{AF}=0.5$) for ferromagnetic coupling [(a)–(c)], 90° coupling [(d)–(f)] and antiferromagnetic coupling [(g)–(i)], with a distribution of in-plane fourfold anisotropy.

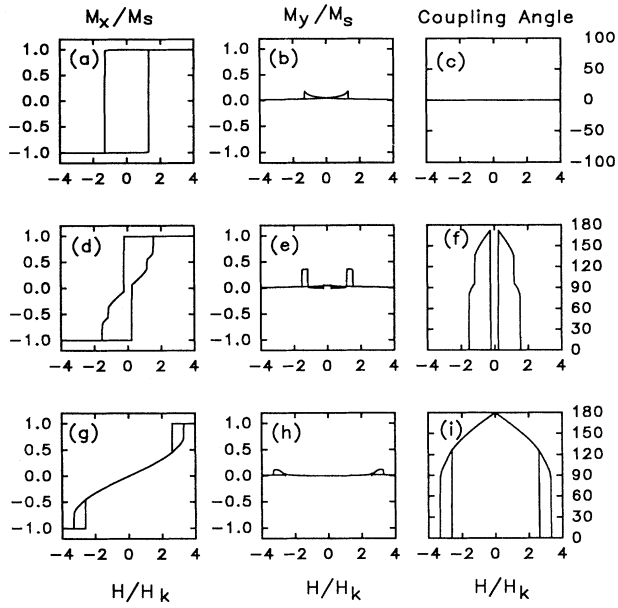

FIG. 10. Compound longitudinal hysteresis loops and interfilm coupling angle between two adjacent ferromagnetic layers during switching processes ($H_{ex}/H_k=3$ and $J_F/J_{AF}=0.5$) for ferromagnetic coupling [(a)–(c)], 90° coupling [(d)–(f)], and antiferromagnetic coupling [(g)–(i)], with easy axes along the x direction.

fourfold anisotropy) and in Figs. 10(a)–10(i) (easy-axis loops). The compound longitudinal hysteresis loops and the coupling angle between the films during the switching process ($H_{ex}/H_k=3$ and $J_F/J_{AF}=0.5$) are shown for ferromagnetic coupling (a)–(c) (AF coupling percentage $a<30\%$), 90° coupling (d)–(f) ($30\%<a<60\%$), and antiferromagnetic coupling (g)–(i) ($60\%<a<100\%$). The coupling angle curves (c), (f), and (i) display the difference in orientation between the magnetization in the layers and clearly show three minimum energy states for ferromagnetic coupling, 90° coupling, and antiferromagnetic coupling. Cubic fourfold in-plane anisotropy describes magnetization reorientation processes better than the uniaxial anisotropy does, and a distribution of anisotropy directions produces more realistic hysteresis loops, as compared with our MOKE measurements. The crude model is not intended to yield actual (measured) hysteresis loops, but rather to indicate the possibility of different coupling regimes.

It has been suggested[69] that imperfections in the layered structure of Co-Cu multilayers stabilize defects in the films' zero-field magnetic substructures, which in turn degrade the macroscopic physical properties. Horizontal antiphase domain boundaries are the most influential magnetic defects which cause the reduction of $(\Delta R/R)_{ideal}$ in the model propose in Ref. 69. In contrast, our results indicate that 90° orientation of domains within the superlattice stack and the presence of domains within the layer themselves (average distribution of 90° domains) are the main reason for observing the GMR effect in superlattices with imperfect interfaces. If we assume the fraction of the film in some misaligned state with an average angle θ between the magnetization directions is $f(\theta)$ and the fraction of the film remaining in the aligned (ferromagnetic coupled) state is $f_{\uparrow\uparrow}$, then we have $f_{\uparrow\uparrow}+f(\theta)=1$. The total sheet resistance due to the partially aligned films is

$$R_T=f(\theta)R_\theta+f_{\uparrow\uparrow}R_{\uparrow\uparrow}$$
$$=f(\theta)(R_\theta-R_{\uparrow\uparrow})+R_{\uparrow\uparrow}\ , \tag{5}$$

where $R_{\uparrow\uparrow}$ is the resistance of the aligned state. The transverse magnetoresistance[70] in a real system (the full-aligned magnetic film orientation is never achieved[39]) can be calculated using the simple linear relationship as follows:

$$\left[\frac{\Delta R}{R}\right]_{\text{measured}}=\frac{R_T-R_{\uparrow\uparrow}}{R_{\uparrow\uparrow}}=f(\theta)\frac{R_\theta-R_{\uparrow\uparrow}}{R_{\uparrow\uparrow}}$$
$$=f(\theta)\left[\frac{\Delta R}{R}\right]\ . \tag{6}$$

$R_{\uparrow\uparrow}$ is due to scattering from impurity, magnon, phonon, and other dead layers (inactive) and rest of the structure.[71] Here, $R_\theta=\Delta R+R_{\uparrow\uparrow}$ (ΔR is the resistance due to spin-dependent scattering). According to spin-dependent scattering theory,[51] the transmission coefficients of an electron propagating between the two ferromagnetic layers are related to the angle θ ($\theta=\theta_1-\theta_2$) between the magnetization vectors in the two layers as follows:

$$T_{\uparrow\uparrow}=T_{\downarrow\downarrow}=\cos^2(\theta/2)\ , \tag{7}$$

$$T_{\uparrow\downarrow}=T_{\downarrow\uparrow}=\sin^2(\theta/2)\ . \tag{8}$$

This leads to a simple expression for the angular dependence of ΔR (Ref. 70) in the form of

$$\Delta R = (\Delta R_{\uparrow\downarrow})\sin^2(\theta/2) , \tag{9}$$

where $(\Delta R_{\uparrow\downarrow})$ is the resistance of ideal antiferromagnetic coupling due to spin-dependent scattering. Therefore, the giant magnetoresistance in a real system with complex angular coupling due to interfacial roughness can be written as

$$\left[\frac{\Delta R}{R}\right]_{\text{measured}} = f(\theta)\sin^2\left[\frac{\theta}{2}\right]\left[\frac{\Delta R_{\uparrow\downarrow}}{R_{\uparrow\uparrow}}\right] = f(\theta)\sin^2\left[\frac{\theta}{2}\right]\left[\frac{\Delta R}{R}\right]_{\text{ideal}} , \tag{10}$$

where $(\Delta R/R)_{\text{ideal}}$ is the MR value due to AF coupling in ideal AF coupled superlattice. We take the simplest possible interpretation where the superlattice consists solely of 90° oriented regions and ferromagnetically aligned regions. The fraction of the film in the 90° orientation is just twice the normalized (M_y/M_s) curve in Fig. 1 of Ref. 38. Here, $\theta = 90°$ and $\sin^2(\theta/2) = \frac{1}{2}$. Therefore, the expected magnetoresistance is simply the percentage of the film magnetized along M_y multiplied by 0.5 $(\Delta R/R)_{\text{ideal}}$ for a system with ideal AF coupling composed of a given number of multilayers. We apply our 90° coupling factor to the GMR data at room temperature from Ref. 9. The modulated MR data in Fig. 11 (solid circles) are calculated from Eq. (10), where the room-temperature $(\Delta R/R)_{\text{ideal}}$ data was extracted from Ref. 9. $(\Delta R/R)_{\text{ideal}}$ was scaled by an empirical factor of 0.6, in order to account for the fact that the saturation MR increases with the bilayer number n.[72] The computed MR curve fits nicely with the experimental MR oscillation curve (open triangles) for our series of Co/Cu superlattices except that the value of the MR in our sample with Cu spacer thickness of 0.8 nm at the first oscillation peak is strongly suppressed. This modeling implies that the principal reason why the magnetoresistance values of imperfect Co-Cu multilayers fall below some ideal value is the competition between the 180° coupling and the 90° coupling in the regions of AF coupling. This competition leads to the complicated magnetic configuration and domain structure of the superlattices. The effect of interfacial roughness on interlayer coupling masks the 180° coupling and gives rise to 90° coupling. This 90° coupling is the main reason for observing the GMR effect in superlattices with imperfect interfaces.

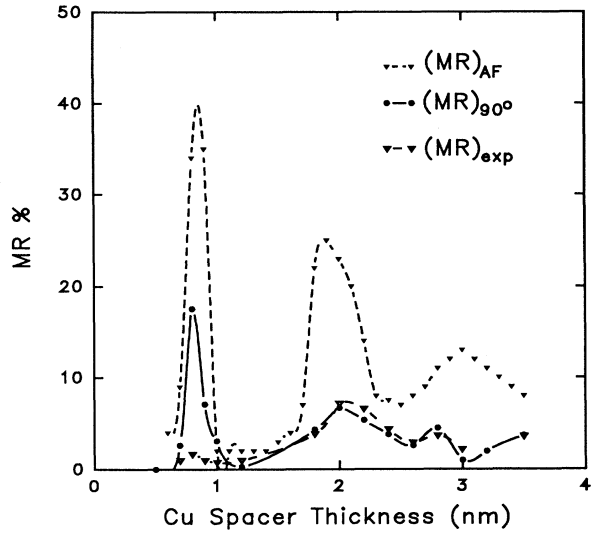

FIG. 11. Saturation MR oscillation curves. The line with solid circles showing GMR oscillation curve is calculated from Eq. (10), the line with closed triangles is MR data at room temperature from Ref. 4, and our 90° coupling MR oscillation curve of the Co/Cu system at room temperature (open triangles) is fitted with the calculated data (solid circles); see text.

TABLE I. Dependence of MR values and saturation resistance R_{sat} at saturation field H_s (14 kOe) on Cu spacer thickness for Si(100)/Co (6 nm)/[Cu(t_{Cu})/Co (1.5 nm)]$_n$/Co (4.5 nm) with n between 6 and 13.

Cu spacer thickness t (nm)	R_{sat} (H_s = 14 kOe) (Ω)	MR (%)
0.7	6.036	0.6
0.8	5.088	1.67
2.0	1.47	7.14
3.5	1.585	3.6

The suppression of the MR value, at the first oscillation position in our superlattice with Cu spacer thickness of 0.8 nm having a wavy layered structure and very rough interfaces, may imply that interface scattering is not favorable in the Co/Cu system to produce high values of MR. As shown in Table I, the resistance R_{sat} at the saturation field increases as the Cu spacer thickness decreases, indicating that the suppression of MR values at the thinnest Cu spacer thicknesses in superlattices with rough interfaces may be caused by diffuse surface scatter,[73] increase of the sheet resistance,[74] and any deleterious effects due to pinhole formation.

IV. DISCUSSION AND CONCLUSION

Giant magnetoresistance and interlayer coupling in Co/Cu superlattices grown on Si(100) oriented crystals. Corning cover glass slides, and holey carbon film covered grids in a dual-beam electron evaporation chamber have been investigated with MOKE, SAXS, LAXS, RBS, cross-section TEM, and STEM electron holography domain observation. LAXS and SAXS profiles and TEM images have shown that the superlattices are polycrystalline, having fcc (111) orientation with coherent grain-to-grain epitaxy and an average grain size ranging from 10 to 14 nm. The superlattices have well-defined layered structures with interfacial roughness of ±0.2–0.4 nm. The magnetotransport measurements show that the magnetoresistance oscillates with a period of about 1 nm as a function of the Cu spacer-layer thickness. The magnitude of the component of the magnetization perpendicular to the applied magnetic-field direction oscillates with the same period. The total magnetization, calculated from the two in-plane hysteresis loops, is used to determine that 90° domains are formed between ferromagnetic

Co layers across the Cu spacer layers in the superlattices, confirmed with domain observation from STEM electron holography. The correlations between the oscillation curves of the 90° magnetization and magnetoresistance suggest that the giant magnetoresistance in superlattices with imperfect interfaces results from the 90° orientation of domains within adjacent Co layers. An interfacial roughness coupling model, based on a modified Ruderman-Kittel-Kasuya-Yosida theory, is proposed for interpreting GMR values and 90° interlayer coupling. The model implies that the principal reason why the magnetoresistance values of imperfect Co/Cu multilayers fall below some ideal value is the competition between the 180° coupling and the 90° coupling in the regions of AF coupling. This competition leads to the complicated magnetic configuration and domain structure of superlattices. It can be concluded that the effect of interfacial roughness on interlayer coupling constants masks the 180° coupling and gives rise to the 90° domain formation. Measured GMR values in superlattices with 90° domain orientation are modulated by an oscillatory factor due to 90° orientation of domains within adjacent Co layers. Magnetoresistance values measured at room temperature and at 77 K from the superlattice Si(100)/Co (6 nm)/[Cu (2 nm)/Co (1.5 nm)]$_8$/Co(4.5 nm) with the Cu spacer-layer thickness at the second oscillation peak are 7% and 14%, respectively.

It has been reported[72,75] that the GMR value in sputtered superlattices depends strongly on the bilayer number. We grew films that were sufficiently thin so as to be electron transparent to 100 keV electron beams so that we could characterize the magnetic microstructure using electron holographic methods. Figure 12 shows the dependence of the GMR value on the bilayer number n for our GMR superlattices of Si(100)/Co (6 nm)/[Cu (2 nm)/Co (1.5 nm)]$_n$ /Co (4.5 nm) as n increases from 2 to 8. Our modest values of GMR could be the result of the small bilayer number n in our samples and our choice of t_{Co} of 1.5 nm. Our GMR values are not that different from those reported in Refs. 22–25, where the suppression of the first oscillation peak at the Cu spacer-layer thickness of 1.0 nm was also observed.

Further, the interfacial roughness of ±0.2–0.4 nm estimated from SAXS data and TEM images is reasonable and can be used in our theoretical model to set an upper limit on the intrinsic coupling strength. The minimum

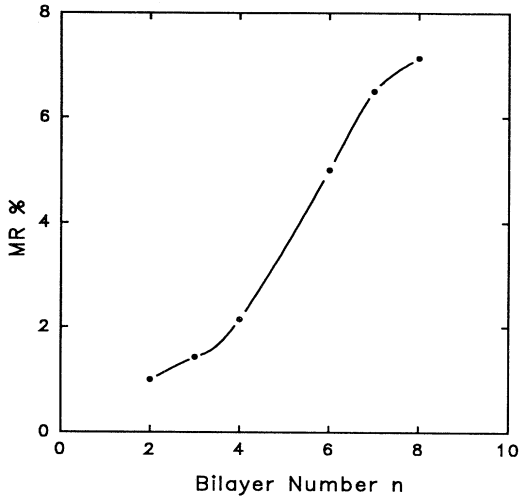

FIG. 12. Dependence of GMR value on the bilayer number n in the series of superlattices Si(100)/Co (6 nm)/[Cu (2 nm)/Co (1.5 nm)]$_n$/Co (1.5 nm)]$_n$ /Co (4.5 nm), showing that the GMR value increases with the bilayer number n.

Cu spacer-layer for our superlattices, corresponding to a layer structure in which each Co atomic layer is atomically close the adjacent Co layers, is approximately 0.8 nm. In this case, strong 90° coupling is still present at the first oscillation maximum even though the value of the MR is strongly suppressed, suggesting that the effects of the spin-dependent density of states on the GMR scattering mechanism are quenched in the limit of very thin spacer layers.[76]

ACKNOWLEDGMENTS

We would like to acknowledge Marion Mankos for the electron holographic images and K. Weiss and D. J. Smith for the transmission electron microscope images. We acknowledge the Center for High Resolution Electron Microscopy at Arizona State University, Grant No. DMR-93-14326. We thank Ann Yates for the x-ray data obtained on equipment purchased under Grant No. NSF-DMR-8406823. This work is supported by the Office of Naval Research under Grant No. N00014-93-1-0099. Finally, we thank Gary Hembree and Kevin Heim for technical assistance and thoughtful discussions.

[1]M. N. Baibich, J. M. Broto, A. Fert, F. Nguyen Van Dau, F. Petroff, P. Etienne, G. Creuzer, A. Friederich, and J. Chazelas, Phys. Rev. Lett. **61**, 2472 (1988).

[2]S. S. P. Parkin, N. More, and K. P. Roche, Phys. Rev. Lett. **64**, 2304 (1990).

[3]P. Grunberg, J. Barnas, F. Saurenbach, J. A. Fuss, A. Wolf, and M. Vohl, J. Magn. Magn. Mater. **93**, 58 (1991).

[4]D. H. Mosca, F. Petroff, A. Fert, P. A. Schroeder, W. P. Pratt, Jr. and R. Laloee, J. Magn. Magn. Mater. **94**, L1 (1991).

[5]S. S. P. Parkin, Phys. Rev. Lett. **67**, 3598 (1991).

[6]E. E. Fullerton, M. J. Conover, J. E. Mattson, C. H. Sowers, and S. D. Bader, Phys. Rev. B **48**, 15 755 (1993).

[7]E. E. Fullerton, M. J. Conover, J. E. Mattson, C. H. Sowers, and S. D. Bader, J. Appl. Phys. **75**, 6461 (1994).

[8]C. D. Potter, R. Schad, P. Belien, G. Verbanck, V. V. Moshchalkov, Y. Bruynseraede, M. Schafer, R. Schafer, and P. Grunberg, Phys. Rev. B **49**, 16 055 (1994).

[9]S. S. P. Parkin, R. Bhadra, and K. P. Roche, Phys. Rev. Lett. **66**, 2152 (1991).

[10]A. Fert, A. Barthelemy, P. Etienne, S. Lequien, R. Loloee, D. K. Lottis, D. H. Mosca, F. Petroff, W. P. Pratt, and P. A. Schroeder, J. Magn. Magn. Mater. **104-107**, 1712 (1992).

[11]M. T. Johnson, P. H. J. Bloemen, R. Coehoorn, J. J. de Vries, N. W. E. McGee, R. Jungblut, A. Reinders, and J. ann de Stegge, in *Magnetic Ultrathin Films: Multilayers and Surfaces/Interfaces and Characterization,* edited by B. T. Jonker *et al.* MRS Symposia Proceedings No. 313 (Materials Research Society, Pittsburgh, 1993), p. 211.
[12]P. H. J. Bloemen, R. van Dalen, W. J. M. Jonge, M. T. Johnson, and J. aan de Stegge, J. Appl. Phys. **73**, 5972 (1993).
[13]P. M. Levy, K. Ounadjela, S. Zhang, Y. Wang, C. B. Sommers, and A. Fert, J. Appl. Phys. **67**, 5914 (1990).
[14]J. Mathon, D. M. Edwards, R. B. Muniz, and M. S. Phan, J. Magn. Magn. Mater, **104-107**, 1712 (1992).
[15]K. B. Hathaway and J. R. Cullen, J. Magn. Magn. Mater. **104-107**, 1840 (1992).
[16]P. Bruno and C. Chappert, Phys. Rev. Lett. **67**, 1602 (1991); Phys. Rev. B **46**, 261 (1992).
[17]J. Mathon, M. Villeret, D. M. Edwards, and R. B. Muniz, J. Magn. Magn. Mater. **121**, 2423 (1993).
[18]P. M. Levy, S. Zhang, and A. Fert, Phys. Rev. Lett. **65**, 1643 (1990).
[19]S. Zhang and P. M. Levy, Phys. Rev. B **47**, 6776 (1993).
[20]Peter M. Levy and Shufeng Zhang, J. Magn. Magn. Mater. **93**, 67 (1991).
[21]P. M. Levy, H. E. Camblong, and S. Zhang, J. Appl. Phys. **75**, 7076 (1994).
[22]J. L. Duvail, A. Fert, L. G. Pereira, and D. K. Lottis, J. Appl. Phys. **75**, 7070 (1994).
[23]F. Giron, P. Boher, Ph. Houdy, F. Pierre, P. Beauvillain, C. Chappert, K. Le Dang, and P. Vieillet, J. Magn. Magn. Mater. **104-107**, 1887 (1992).
[24]F. Giron, P. Boher, Ph. Houdy, P. Beauvillain, C. Chappert, K. Le Dang, and P. Vieillet, J. Magn. Magn. Mater. **121**, 318 (1993).
[25]P. P. Freitas, I. G. Trindade, L. V. Melo, J. L. Leal, N. Barradas, and J. C. Soares, J. Appl. Phys. **73**, 5527 (1993).
[26]J. J. de Miguel, A. Cebollada, J. M. Gallego, R. Miranda, C. M. Schneider, P. Schuster, and J. Kirschner, J. Magn. Magn. Mater. **93**, 1 (1991).
[27]M. Ruhrig, R. Schafer, A. Hubert, R. Mosler, J. A. Wolf, S. Demokritov, and P. Grunberg, Phys. Status Solidi A **125**, 635 (1991).
[28]J. Unguris, R. J. Celotta, and D. T. Pierce, J. Appl. Phys. **75**, 6437 (1994).
[29]M. E. Filipkowski, C. J. Gutierrez, J. J. Krebs, and G. A. Prinz, J. Appl. Phys. **73**, 5963 (1993).
[30]Z. Celinski, B. Heinrich, and J. F. Cochran, J. Appl. Phys. **73**, 5966 (1993).
[31]J. C. Slonczewski, J. Appl. Phys. **73**, 5957 (1993).
[32]J. C. Slonczewski, Phys. Rev. Lett. **67**, 3172 (1991).
[33]R. Ribas and B. Dieny, J. Magn. Magn. Mater. **121**, 313 (1993).
[34]R. P. Erickson, K. B. Hathaway, and J. R. Cullen, Phys. Rev. B **47**, 2626 (1993).
[35]R. P. Erickson, J. Appl. Phys. **75**, 6163 (1994).
[36]J. Barnas and P. Grunberg, J. Magn. Magn. Mater. **123**, L21 (1993).
[37]K. Brohl, S. diNunzio, F. Schreiber, Th. Zeidler, and H. Zabel, J. Appl. Phys. **75**, 6184 (1994).
[38]Z. J. Yang and M. R. Scheinfein, Appl. Phys. Lett. **66**, 236 (1995).
[39]Y. U. Idzerda, C.-T. Chen, S. F. Cheng, W. Vavra, G. A. Prinz, G. Meigs, H.-J. Lin, and G. H. Ho (unpublished).
[40]S. S. P. Parkin *et al.*, Appl. Phys. Lett. **58**, 2710 (1991).
[41]Robert J. Culbertson and Barry J. Wilkens (unpublished).
[42]B. D. Cullity, *Elements of X-ray Diffraction,* 2nd ed. (Addison-Wesley, Reading, MA, 1978), p. 86; *X-ray Diffraction Procedures for Polycrystalline and Amorphous Materials,* edited by Harold P. Klug and Leroy E. Alexander (Wiley, New York, 1974); E. M. Gyorgy, D. B. McWhan, J. R. Walker, Jr., and L. R. Waszcak, Phys. Rev. B **25**, 6739 (1982).
[43]E. Spiller, Rev. Phys. Appl. **23**, 1727 (1988).
[44]F. Rieutord, J. J. Benattar, L. Bosio, P. Robin, C. Blot, and R. de Kouchkovsky, J. Phys. (Paris) **48**, 679 (1987).
[45]P. Croce and L. Nevot, Rev. Phys. Appl. **11**, 113 (1976).
[46]J.-F. Bobo, B. Baylac, L. Hennet, O. Lenoble, M. Piecuch, B. Raquet, J.-C. Oussett, J. Magn. Magn. Mater. **121**, 291 (1993); M. J. Pechan, J. F. Aukner, C. F. Majkrazk, D. M. Kelley, and I. K. Schuller, J. Appl. Phys. **75**, 6178 (1994).
[47]G. Rupp and K. Schuster, J. Magn. Magn. Mater. **121**, 416 (1993).
[48]David J. Smith, Z. G. Li, A. R. Modak, S. S. P. Parkin, R. F. C. Farrow, and R. F. Marks, Scr. Metall. Mater. **30**, 689 (1994).
[49]A. R. Modak, David J. Smith, and S. S. P. Parkin, Phys. Rev. B **50**, 4232 (1994).
[50]A. Cebollada, J. L. Martinez, J. M. Gallego, J. J. de Miguel, R. Miranda, S. Ferrer, F. Batallan, G. Fillion, and J. P. Rebouillat, Phys. Rev. B **39**, 9726 (1989).
[51]R. E. Camley and J. Barnas, Phys. Rev. Lett. **63**, 664 (1989).
[52]Roy Clarke, Daryl Barlett, Frank Tsui, Baoxing Chen, and Ctirad Uher, J. Appl. Phys. **75**, 6174 (1994).
[53]Z. J. Yang and M. R. Scheinfein, J. Appl. Phys. **74**, 6810 (1993).
[54]E. R. Moog, C. Lui, S. D. Bader, and J. Zak, Phys. Rev. B **39**, 6949 (1989).
[55]R. Mattheis, W. Andra, L. Fritzsch, J. Langer, and S. Schmidt (unpublished).
[56]M. Mankos, M. R. Scheinfein, and J. M. Cowley, J. Appl. Phys. **75**, 7418 (1994); Ultramicrosc. **58**, 87 (1995).
[57]M. Mankos, Z. J. Yang, M. R. Scheinfein, J. M. Cowley, IEEE Trans. Magn. **30**(6), 4497 (1994).
[58]L. J. Heyderman, J. N. Chapman, and S. S. P. Parkin, J. Phys. D **27**, 881 (1994).
[59]D. Greig, M. J. Hall, C. Hammon, B. J. Hickey, H. P. Ho, M. A. Howson, M. J. Walker, N. Wiser, and D. G. Wright, J. Magn. Magn. Mater. **110**, L239 (1992).
[60]J. P. Renard, P. Beauvillain, C. Dupas, K. Le Dang, P. Veillet, E. Vélu, C. Marlière, and D. Renard, J. Magn. Magn. Mater. **115**, L147 (1992).
[61]J. Kohlhepp, S. Cordes, H. J. Elmers, and U. Gradmann, J. Magn. Magn. Mater. **111**, L231 (1992).
[62]A. Schreyer, K. Bröhl, J. F. Ankner, C. F. Majkrzak, T. Zeidler, P. Bödeker, N. Metoki, and H. Zabel, Phys. Rev. B **47**, 15 334 (1993).
[63]W. F. Egelhoff, Jr. and M. T. Kief, Phys. Rev. B **45**, 7795 (1992).
[64]R. F. Marks, R. F. C. Farrow, S. S. P. Parkin, C. H. Lee, B. D. Hermsmeier, C. J. Chien, and S. B. Hagstrom, in *Heteroepitaxy of Dissimilar Materials,* edited by R. F. C. Farrow *et al.*, MRS Symposia Proceedings No. 221 (Materials Research Society, Pittsburgh, 1991), p. 15.
[65]U. Gradmann, H.-J. Elmer, and J. Kohlhepp, in *Magnetic Ultrathin Films: Multilayers and Surfaces/Interfaces and Characterization* (Ref. 11), p. 15.
[66]B. Dieny, J. P. Gavigan, and J. P. Rebouillat, J. Phys. Condens. Matter **2**, 159 (1990).
[67]B. Heinrich, J. F. Cochran, M. Kowalewski, J. Kirschner, Z.

Celinski, A. S. Arrott, and K. Myrtle, Phys. Rev. B **44**, 9348 (1991).
[68]K. Bröhl, Th. Zeidler, F. Schreiber, A. Schreyer, and H. Zabel, J. Magn. Magn. Mater. 130, L1 (1994).
[69]R. J. Highmore, J. E. Evetts, and R. E. Somekh, J. Magn. Magn. Mater. **123**, L13 (1993).
[70]A. Chaiken, G. A. Prinz, and J. J. Krebs, J. Appl. Phys. **67**, 4892 (1990).
[71]B. Dieny, P. Humbert, V. S. Sperious, S. Metin, B. A. Gurney, P. Baumgart, and H. Lefakis, Phys. Rev. B **45**, 806 (1992).
[72]S. S. P. Parkin, Anjenaya Modak, and David J. Smith, Phys. Rev. B **47**, 9136 (1993).
[73]T. S. Plaskett and T. R. McGuire, J. Appl. Phys. **73**, 6378 (1993).
[74]X. Bian, J. O. Ström-Olsen, Z. Altounian, Y. Huai, and R. W. Cochrane, J. Appl. Phys. **75**, 7064 (1994).
[75]T. S. Plaskett and T. R. McGuire, J. Appl. Phys. **73**, 6378 (1993).
[76]Roy Clarke, Darryl Barlett, Frank Tsui, Baoxing Chen, and Ctirad Uher, J. Appl. Phys. **75**, 6174 (1994).

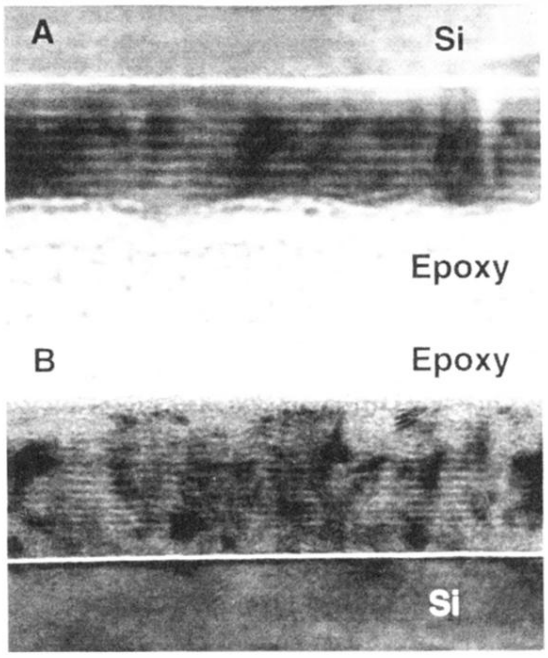

FIG. 5. (a) Cross-section transmission electron micrograph of Co/Cu multilayer with nominal structure Si(100)/Co (6 nm)/[Cu (2 nm)/Co (1.5 nm)]$_8$/Co (4.5 nm). The brightest layer is native oxide SiO, the top of the image is Si substrate, and the bottom is epoxy mount. The dark layers are Cu spacer layers. (b) Cross-section transmission electron micrograph of Co/Cu multilayer with nominal structure Si(100)/Co (6 nm)/[Cu(0.8 nm)/Co (1.5 nm)]$_{13}$/Co (4.5 nm), illustrating a wavy layered structure when the Cu spacer layer is very thin.

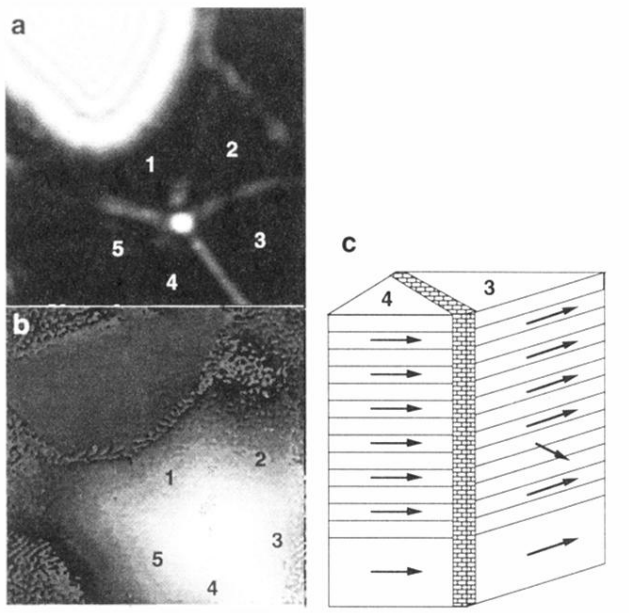

FIG. 6. Domain structure for the superlattice with a nominal structure of Co(6 nm)/[Cu (3 nm)/Co (1.5 nm)]$_6$/Cu(3 nm)]. (a) Fresnel image (2.8 μm across). The domains are numbered 1–5, respectively. (b) Absolute mode STEM electron holographic phase image; (c) A proposed domain structure in the region of the superlattice imaged in (a), indicating the presence of 90° domain formation within the superlattices stack, and the presence of domains within the layers themselves.